Rheology of Block Copolypeptide Solutions: Hydrogels with Tunable Properties

Victor Breedveld,*,†,‡,§ Andrew P. Nowak,†,|| Jun Sato,§ Timothy J. Deming,†,|| and David J. Pine†,‡

Materials Research Laboratory, Department of Chemical Engineering, and Departments of Materials and Chemistry, University of California, Santa Barbara, California 93106 and School of Chemical & Biomolecular Engineering, Georgia Institute of Technology, Atlanta, Georgia 30332

Received January 14, 2004; Revised Manuscript Received March 14, 2004

ABSTRACT: Amphiphilic block copolypeptides were prepared through transition-metal-mediated polymerization of amino acid *N*-carboxyanhydrides. In aqueous solution these materials form strong hydrogels at low concentrations. The self-assembly process that is responsible for gelation was investigated by measuring the rheological properties of the gels for a variety of molecular architectures: poly-L-lysine-*b*-poly-L-leucine diblock and poly-L-lysine-*b*-poly-L-leucine-*b*-poly-L-lysine triblock copolypeptides. Experiments showed that the rodlike helical secondary structure of enantiomerically pure poly-L-leucine blocks was instrumental for gelation at polypeptide concentrations as low as 0.25 wt %. The hydrophilic polyelectrolyte segments have stretched coil configurations and stabilize the twisted fibril assemblies by forming a corona around the hydrophobic core. The self-assembly of hydrophobic blocks is highly specific and sensitive to the chirality of the helices. It was found that mechanical properties of the gels can be tuned through the molecular architecture of the block copolypeptides and also by carefully mixing different polypeptides in solution.

I. Introduction

Self-assembly of block copolymers is an excellent tool to manipulate the structure and rheology of polymer melts and solutions.[1] In melts, the interaction between the different blocks tends to drive the system toward phase separation into homogeneous regions, but geometrical limitations due to the *intra*molecular bonds between blocks of different physicochemical nature prevent macroscopic phase separation and lead to a zoology of morphologies.[2,3] The phase behavior is largely controlled by molecular architecture: number of blocks, monomer composition of blocks, and relative lengths of the blocks. In block copolymer solutions the interaction between polymer and solvent adds an extra dimension, especially when the solvent is selective: a poor solvent for at least one of the blocks and a good solvent for the others.

An important class is formed by aqueous solutions of amphiphilic block copolymers that consist of hydrophobic and hydrophilic blocks. Analogous to smaller surfactant molecules, amphiphilic block copolymers self-assemble in an aqueous environment in order to minimize contact between hydrophobic segments and water. The morphology of the resulting microstructure depends heavily on molecular architecture and can range from spherical micelles to cubic, hexagonal, and lamellar phases.[4,5] In the presence of a second, apolar liquid, the ternary phase diagram is even more complicated, including gyroid structures.[6] The strong dependence of self-assembly on molecular design implies that in order to achieve optimum structural control the block copolymers must have a narrow polydispersity, not only with respect to total molecular weight, but also regarding the length of individual blocks.

We report on the rheology of a novel class of block copolymers: amphiphilic block copolypeptides. Recent development of transition-metal-mediated polypeptide synthesis by Deming[7,8] has provided access to this interesting class of synthetic biomimetic materials. The versatility of the polymerization reaction, in particular the ability to incorporate a large variety of amino acid monomers, both natural and synthetic, results in unprecedented flexibility of molecular design. Monomer species are formed by converting α-amino acids into α-amino-*N*-carboxyanhydrides (NCA). These NCAs are then polymerized through a transition-metal-mediated ring-opening polymerization to yield polypeptide. Subsequent batchwise addition of different NCA monomers leads to multiblock architectures with well-defined block lengths and low polydispersity (see Materials section).

Even within each block there is control over the design: blocks can be either homogeneous or statistically random heterogeneous sequences of amino acid mixtures. Thus, monomers with specific (bio)chemical properties can be incorporated along the polypeptide backbone to mimic biological functionality or induce specific chemical reactivity. Block copolypeptides also offer a unique parameter to manipulate structure on the molecular level: the ability of peptides to fold into intramolecular secondary structures, α-helix and *β*-strand. This level of structural control is specific for peptides and leads to intriguing material properties.

Block copolypeptides do not have the complex composition and perfect sequence control found in natural proteins and synthetic oligopeptides produced with recombinant DNA or solid-state techniques.[9−11] Instead, they form a separate class of molecular building blocks that possess some of the unique features of natural polypeptides. The synthesis, however, is accurate, flex-

* To whom correspondence should be addressed. E-mail: victor.breedveld@chbe.gatech.edu.
† Materials Research Laboratory, University of California, Santa Barbara.
‡ Department of Chemical Engineering, University of California, Santa Barbara.
§ Georgia Institute of Technology.
|| Departments of Materials and Chemistry, University of California, Santa Barbara.

10.1021/ma049885f CCC: $27.50
Published on Web 04/24/2004

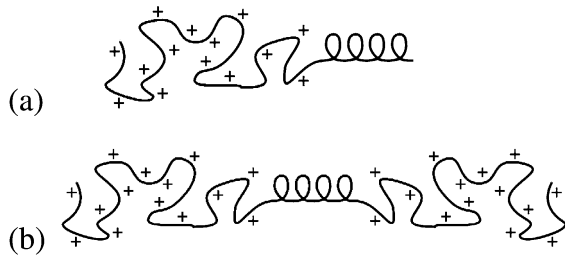

Figure 1. (a) Diblock and (b) triblock copolypeptide architecture; the hydrophobic leucine block exhibits α-helical secondary structure, and the charged polyelectrolyte block has a stretched coil configuration.

ible, and readily scalable for production of greater than gram quantities of material. These characteristics enable systematic studies of intermolecular interactions, and in that respect the block copolypeptides can be seen as a rudimentary model system for protein−protein interaction.

Here we focus on the rheological properties of aqueous solutions of amphiphilic di- and triblock copolymers. The diblock copolymers consist of a hydrophilic polyelectrolyte block (poly-L-lysine, K) and a shorter hydrophobic block (poly-L-leucine, L; see Figure 1a). L-Leucine is a strong α-helix former, and we have shown previously that the helical structure is stable for leucine block lengths of at least 20 monomers. The presence of secondary structure is instrumental for the formation of stiff hydrogels by these materials at low polypeptide concentrations.[12] Here we elucidate the gelation mechanism in more detail by systematically varying the molecular architecture and studying the rheological properties of the hydrogels.

The classical self-assembly mechanism for amphiphilic diblock copolymers is the formation of micelles. Micellar systems generally exhibit elastic gel properties only when the concentration of micelles is high enough to pack them into ordered arrays, which typically requires at least 5−10 wt % of polymer.[13,14] In contrast, our most efficient polypeptide gel formers form elastic gels at concentrations as low as 0.25 wt %. One way to induce gelation in micellar systems is the presence of an attractive interaction between the hydrophilic coronas. "Sticky" micelles have been generated from PAA-PS block copolymers where part of the polyacrylic ester precursor was not hydrolyzed into hydrophilic polyelectrolyte PAA residues and these remaining hydrophobic entities act as "stickers" between micelles.[1] As a result of the attractive forces, the micelles aggregate into a fractal network with elastic properties. The hydrophilic blocks of our block copolypeptides consist of positively charged poly-L-lysine, which should generate repulsion rather than attraction; this seemingly obvious conclusion is illustrated by the fact that solutions of poly-L-lysine homopolymer remain viscous liquids even at high concentrations. Therefore, other intermolecular forces must be responsible for self-assembly into hydrogels at low polypeptide concentrations. CryoTEM imaging has suggested the formation of extended fibrils or membranes on the molecular length scale, directed by the secondary structure of the hydrophobic block.[12,15]

As part of the investigation we also explored triblock architectures with a hydrophobic core and two polyelectrolyte end groups (Figure 1b). This design fundamentally differs from the more common telechelic copolymers, where a hydrophilic polymer is functionalized with two hydrophobic endcaps. These more common telechelic polymers generally form flowerlike micelles with hydrophobic cores. However, the hydrophobic segments of some of the polymer strands can form bridges between different micelles. With increasing polymer concentration, the bridging generates a percolated network with elastic properties.[16,17] The network arises from the fundamental feature that each molecule possesses *two* associative end groups, thus facilitating the formation of large structures. Many biopolymers form strong gels at low concentrations in a similar way: along their backbone they have *multiple* associative sites that can form physical links with other polymer molecules. Gelatin is a well-known example in which the intermolecular connections are formed by triple-helix configurations involving three different molecules.[18] The di- and triblock copolypeptides in this study lack such an obvious mechanism for the formation of a mechanically supporting interconnected network at low concentrations.

II. Experimental Section

Materials. The amphiphilic di- and triblock copolypeptides K_nL_m and $K_nL_mK_n$ in this paper consist of blocks of poly(L-lysine·HBr) (abbreviated as K_n, *n* being the number of monomers in the block) and poly(L-leucine) (L_m). In one case the D-enantiomers of lysine and leucine were used; the resulting block copolypeptide is referred to as D-$K_{160}L_{40}$. In addition, a polymer was synthesized with L-lysine and a statistical racemic mixture of D/L-leucine in the hydrophobic leucine block, designated K_{160}(rac-L)$_{40}$. The subscripts in the notations K_nL_m and $K_nL_mK_n$ refer to the predicted block lengths, based on monomer to initiator feed ratios and tandem GPC/light-scattering. Below, a detailed description of the synthesis procedures is given for a representative diblock and triblock copolypeptide: $K_{160}L_{40}$ and $K_{180}L_{40}K_{180}$.

Poly(Nϵ-CBZ-L-lysine)$_{160}$-*block*-poly(L-leucine)$_{40}$. In the drybox Nϵ-CBZ-L-lysine NCA (1.00 g, 3.27 mmol) was weighed out and dissolved in THF (20 mL) in a 100 mL flask. Co(PMe$_3$)$_4$ (29.7 mg, 81.8 μmol) was weighed out and dissolved in THF (∼2 mL). The solution was then injected into the Nϵ-CBZ-L-lysine NCA mixture through a glass pipet. Immediately after addition of the Co(PMe$_3$)$_4$ complex, the flask was vigorously swirled and left to stand for approximately 45 min. An aliquot was then removed for FTIR analysis to ensure consumption of NCA monomer (1790, 1854 cm^{-1}) and formation of amide bonds from the polypeptide backbone (1650, 1540 cm^{-1}). Once all Nϵ-CBZ-L-lysine NCA was consumed, L-leucine NCA (128.3 mg, 0.818 mmol) was weighed out, dissolved in THF (2−3 mL), and added to the solution via pipet. After 1 h another aliquot of solution was removed, and consumption of L-leucine NCA was verified with IR. The 100 mL flask was transferred out of the drybox, and polymer was precipitated using diethyl ether. M_n = 47 800, PDI = 1.28.

Poly(L-lysine HBr)$_{160}$-*block*-poly(L-leucine)$_{40}$. In a 100 mL flask with a stir bar, poly(Nϵ-CBZ-L-lysine)$_{160}$-*block*-poly(L-leucine)$_{40}$ was dissolved in trifluoroacetic acid (40 mL). Once all polymer was in solution, an ice bath was placed under the flask and excess 33 wt % HBr in acetic acid was added via pipet (∼2.7 mL, 5 equiv per CBZ group). The flask was loosely capped to accommodate the gas evolved and left to stir for 1 h. After this time, diethyl ether (60 mL) was added to precipitate any polymer still remaining in solution. The suspension of precipitated polymer was poured into 50 mL centrifuge tubes and spun down and decanted, and the pellet at the bottom of the tube was transferred back to the flask, where the entire mass could be washed with diethyl ether. Deionized water (40 mL) and LiBr (∼250 mg) were added to the polymer and vigorously stirred. After 30 min the solution and any undissolved polymer still remaining were transferred to a dialysis bag (Regenerated Cellulose, Spectrapor, MWCO 6−8 kDa) that was placed in a 4 L container of deionized water. Over the next 3 days the water was exchanged 2−3 times per

day. The solution was then transferred to a beaker, where it was frozen and placed on a freeze dryer to yield the product as a white spongy material. Typical yields were between 80% and 90%, and remaining CBZ groups were below 3% as verified by ^{1}H and ^{13}C NMR.

Poly(Nϵ-CBZ-L-lysine)$_{180}$-*block*-poly(L-leucine)$_{40}$-*block*-poly(Nϵ-CBZ-L-lysine)$_{180}$. In the drybox Nϵ-CBZ-L-lysine NCA (0.500 g, 1.63 mmol) was weighed out, transferred to a 100 mL flask, and dissolved in THF (10 mL). Co(PMe$_3$)$_4$ (13.2 mg, 36.2 μmol) was weighed out, dissolved in THF (~2 mL), and injected into the solution using a glass pipet. Immediately after addition of the Co(PMe$_3$)$_4$ complex, the flask was vigorously swirled and left to stand for approximately 45 min. An aliquot was then removed for FTIR analysis to ensure consumption of NCA monomer (1790, 1854 cm^{-1}) and formation of amide bonds from the polypeptide backbone (1650, 1540 cm^{-1}). Once all Nϵ-CBZ-L-lysine NCA was consumed, L-leucine NCA (57.0 mg, 0.363 mmol) was weighed out, dissolved in THF (2−3 mL), and added to the solution via pipet at a ratio of 10 mol % of total NCA monomer. After 1 h another aliquot of solution was removed, and consumption of L-leucine NCA was verified with FTIR. Finally, Nϵ-CBZ-L-lysine NCA (0.500 g, 1.63 mmol) was again weighed out and dissolved in 10 mL of THF. This was transferred to the polymerization mixture by pipet, and complete block addition was tested with FTIR after 1 h. The 100 mL flask was transferred out of the drybox, and polymer was precipitated using diethyl ether.

Poly(L-lysine HBr)$_{180}$-*block*-poly(L-leucine)$_{40}$-*block*-poly(L-lysine HBr)$_{180}$. In a 100 mL flask with a stir bar, poly(Nϵ-CBZ-L-lysine)$_{180}$-*block*-poly(L-leucine)$_{40}$-*block*-poly(Nϵ-CBZ-L-lysine)$_{180}$ was dissolved in trifluoroacetic acid (40 mL). Once all polymer was in solution, an ice bath was placed under the flask and excess 33 wt % HBr in acetic acid was added via pipet (~2.7 mL, 5 equiv per CBZ group). The flask was loosely capped to accommodate the gas evolved and left to stir for 1 h. After this time diethyl ether (60 mL) was added to precipitate any polymer still remaining in solution. The suspension of precipitated polymer was poured into 50 mL centrifuge tubes and spun down. The liquid was then decanted, and the pellet at the bottom of the tube was transferred back to the flask, where the entire mass could be washed with diethyl ether 2−3 times. Deionized water (40 mL) and LiBr (~250 mg) were added to the polymer and vigorously stirred. After 30 min the solution and any undissolved polymer still remaining were transferred to a dialysis bag (Regenerated Cellulose, Spectrapor, MWCO 6−8 kDa) that was placed in a 4 L container of deionized water. Over the next 3 days the water was exchanged 2−3 times per day. The solution was then transferred to a beaker, where it was frozen and placed on a freeze dryer to yield the product as a white spongy material. Typical yields were between 80% and 90%, and remaining CBZ groups were below 3% as verified by ^{1}H and ^{13}C NMR.

GPC and NMR. Molecular weights were determined using tandem gel permeation chromatography/light scattering performed on an SSI Accuflow Series III liquid chromatograph pump equipped with a Wyatt DAWN/DSP light-scattering detector and Wyatt Optilab DSP. Separations were effected by 10^5, 10^4, and 10^3 A Phenomenex 5 μm columns using 0.1 M LiBr in DMF as effluent at 60 °C. ^{1}H and ^{13}C {^{1}H} NMR spectra were taken on a Bruker 500 MHz spectrometer. All polypeptide NMR samples were run in *d*-TFA (20−50 mg/mL) at 50 °C. Amino acid compositions of the copolymers were found to be within 3% of predicted values. Chain lengths of the copolymers were found to be within 8% of predicted lengths with CLD (weight average length/number average length) ranging between 1.1 and 1.3.

Rheology. Rheological measurements were performed on an ARES-LS1 controlled strain rheometer from Rheometric Scientific (now TA Instruments). Additional studies of the dynamic moduli were carried out on an MCR300 controlled stress rheometer from Paar-Physica. Both instruments were equipped with cone-plate configurations. Two different geometries were used on the ARES: a 50 mm diameter cone with a 2° angle and a 25 mm cone with a 4° angle. The latter geometry is less stress-sensitive because of the smaller diameter but requires a smaller sample volume. The choice between the two geometries was based on a qualitative judgment of the sample properties and the amount of material available: concentrated, gellike samples could be measured with the 25 mm cone, whereas dilute solutions required the sensitivity of the 50 mm cone. For a number of samples both geometries were employed to ensure reproducibility, and excellent agreement was always observed. The MCR300 was operated with a 50 mm diameter 1° cone or with a 25 mm 2° cone.

The rheological properties of all samples were determined through the following measurement protocol. First, an oscillatory strain amplitude sweep (strain amplitude $\gamma_0 = 0.001-10$) at fixed frequency ($\omega = 6$ rad/s) was performed to establish the linear regime. Having established the maximum strain permitted for linear viscoelastic response, an oscillatory frequency sweep (frequency $\omega = 0.01-100$ rad/s) was performed to measure $G'(\omega)$ and $G''(\omega)$, the linear viscoelastic storage and loss modulus, respectively. The strain and frequency sweeps were used to characterize well-rested samples in "equilibrium" as well as to monitor the recovery of gels after their breakdown by large-amplitude oscillatory strain. Between strain amplitude sweeps and frequency sweeps, samples were allowed to rest for several minutes to facilitate sample recovery from the large nonlinear oscillatory deformations. In addition to oscillatory measurements, steady-shear flow curves were also measured.

The recovery measurements were carried out only for samples with gellike properties and consisted of two steps: an initial phase of nonlinear, large-amplitude oscillations to break down the gel structure (typically at $\gamma_0 = 10$ and $\omega = 6$ rad/s for a duration of 600 s), followed by linear small-deformation oscillations at the same angular frequency to monitor recovery of mechanical strength (typically at $\gamma_0 = 0.003$ for 3600 s). Large-amplitude oscillations were the method of choice for breaking down the gel structure as they were more efficient than steady-shear flow, especially for gels having large critical strain amplitudes. The most likely explanation is that there is wall-slip in steady-shear flow; the reversal of direction and variation of shear rate in oscillatory flow help to break down the gels in a more homogeneous manner.

Finally, we note that the rheological measurements were not sensitive to the methods used to prepare the solutions. In general, solutions were prepared by dissolving freeze-dried block copolypeptide samples in deionized water, enhancing the mixing and dissolution process with a vortex mixer. However, identical mechanical properties were obtained by allowing the copolypeptides to dissolve overnight. Samples were left overnight before performing rheological experiments, which was sufficiently long to prevent time dependence.

All rheological measurements were carried out with Peltier thermostating units at 23.5 °C in order to minimize evaporation of the aqueous samples. As noted in previous work,[12] the block copolypeptide gels are highly insensitive to temperature. This observation was corroborated quantitatively by experiments with 3.0 wt % $K_{160}F_{40}$ poly(L-lysine-HBr)-*block*-poly(L-phenylalanine) gel, which is rheologically similar to $K_{160}L_{40}$;[19] temperature variations from 5 to 45 °C did not result in detectable changes in hydrogel rheology.

III. Results and Discussion

Gelation and Gel Rheology. The K_nL_m diblock copolypeptide solutions showed a gelation transition in deionized water at remarkably low polypeptide concentrations. In Figure 2a the dynamic moduli G' and G'' are shown as a function of angular frequency ω for four different concentrations of $K_{170}L_{30}$. Up to 0.50 wt % of polypeptide, the solutions are viscous liquids. The apparent rise of G' at high frequencies for the 0.50 wt % sample is an experimental artifact of the cone-plate geometry on the ARES rheometer (gap loading limit) and is observed for all low-viscosity liquids; therefore,

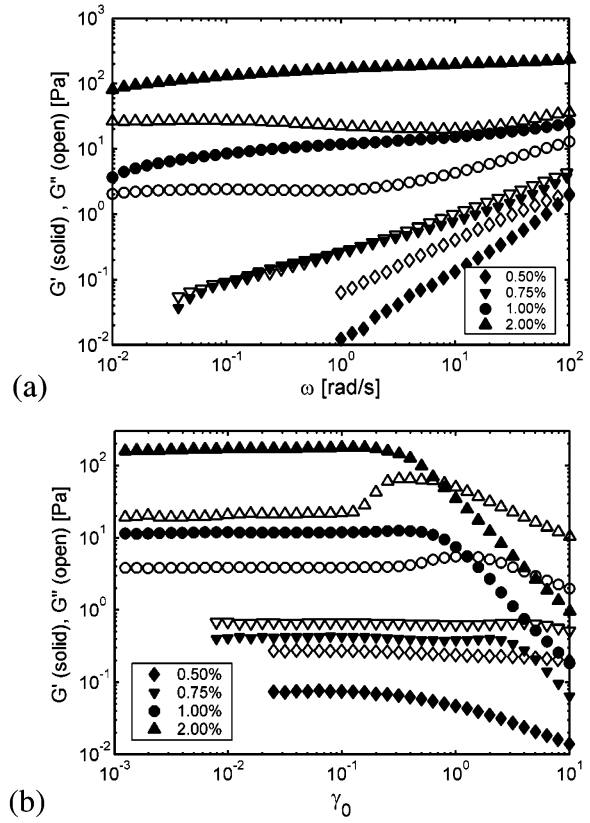

Figure 2. (a) Storage modulus G' (solid symbols) and loss modulus G'' (open symbols) as a function of angular frequency for aqueous $K_{170}L_{30}$ solutions at four different polypeptide concentrations: (◆) 0.50 wt %, (▼) 0.75 wt %, (●) 1.00 wt %, and (▲) 2.00 wt %; (b) Strain sweeps for the same samples at angular frequency $\omega = 6$ rad/s.

it should not be interpreted as a sample relaxation time. At a concentration of 0.75 wt % the $K_{170}L_{30}$ solution goes through a sudden gelation transition, marked by overlapping $G'(\omega)$ and $G''(\omega)$ curves over the entire frequency range. Above this concentration the gels became stronger with the addition of more material.

Strain amplitude sweeps were measured at a fixed angular frequency $\omega = 6$ rad/s and are presented in Figure 2b. In addition to verifying that the measurements reported in Figure 2a were performed well below the limiting strain for linear response, the data in Figure 2b show that the elastic response of the gel, as measured by G', decreases rapidly above a concentration-dependent critical strain amplitude γ_{0c}, indicating a breakdown in the gel network. Moreover, the critical strain amplitude γ_{0c} decreases with increasing polypeptide concentration. Thus, the sample becomes more brittle, in the sense that the gel structure breaks down at smaller strains, as polypeptide concentration increases.

The transient properties of the hydrogels were studied by subjecting the samples to oscillatory strains of sufficiently large amplitude to break down the gel network (i.e., much greater than γ_{0c}) and then following the recovery of elasticity by monitoring G' using much smaller strain amplitudes (much less than γ_{0c}). In Figure 3 the transient recovery of the gel is shown for two gellike $K_{170}L_{30}$ samples, at concentrations of 1.0 and 2.0 wt %, respectively. During the initial 600 s, G' (measured at a large nonlinear strain amplitude) drops by 2 orders of magnitude, below the level of the loss modulus G''. Upon switching to smaller-amplitude

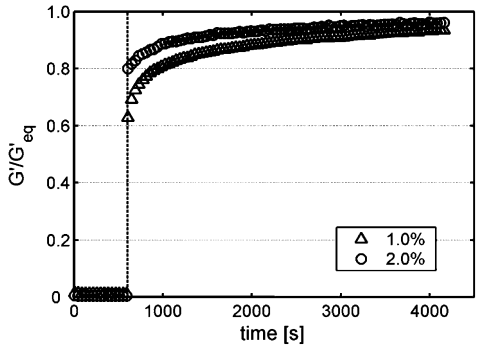

Figure 3. Storage modulus G' as a function of time for aqueous $K_{170}L_{30}$ solutions at (○) 1.0% and (△) 2.0%; during the initial 600 s the gel is broken down through large-amplitude oscillations ($\omega = 6$ rad/s, $\gamma_0 = 10$), and from then on the recovery of gel strength is monitored through small-amplitude oscillations ($\omega = 6$ rad/s, $\gamma_0 = 10$). To facilitate comparison, G' has been normalized to the equilibrium value (see Figure 2a).

strain oscillations, the samples began to recover their elastic properties. The speed of elastic recovery was remarkable; during the brief period (~10 s) that the rheometer needed to switch between strain amplitudes, most of the original gel strength was regained, after which the gel continued to recover its elasticity, albeit at a slower rate, but leading to full recovery with a characteristic time scale of tens of minutes. In the recovery phase, the increase in elastic modulus G' was accompanied by a simultaneous decrease of G'', which suggests that during recovery more and more of the structures in solution are incorporated into the elastic network. For comparison, the same measurement protocol was applied to a 2.0 wt % gelatin solution,[12] and the recovery process was found to have a characteristic time of several hours.

The basic rheological measurements presented above for a representative $K_{170}L_{30}$ block copolypeptide provide some clues about the intermolecular interactions and self-assembled structure. As noted in the Introduction, amphiphilic diblock copolymers usually self-assemble into spherical micelles, driven by the incompatibility of one of the blocks with the solvent. However, for the K_nL_m block copolypeptides, the helical secondary structure of the hydrophobic block causes them to be essentially stiff rods, which introduces geometrical impediments for spherical packing of the molecules. This is illustrated schematically in Figure 4: the geometrical constraints associated with spherically packing stiff rods prevent the hydrophobic blocks from effectively shielding themselves from the water. Lamellar packing of the hydrophobic regions pack the rods more efficiently, but the resulting two-dimensional flat membranes limit the volume available for the hydrophilic polyelectrolyte segments. Moreover, the electrostatic repulsion of polyelectrolyte segments confined to a two-dimensional structure is energetically costly. Hence, extended two-dimensional flat membranes are disfavored energetically for samples with long hydrophilic segments.

Neither spherical micelles nor flat membranes are expected to lead to gel formation at the low concentrations where gelation was observed for $K_{170}L_{30}$ since neither structure is particularly well suited for forming an interconnected three-dimensional network at such low concentrations. The inability of membranes to form gels is supported by the properties of nonionic versions of the lysine-leucine block copolymers, which were

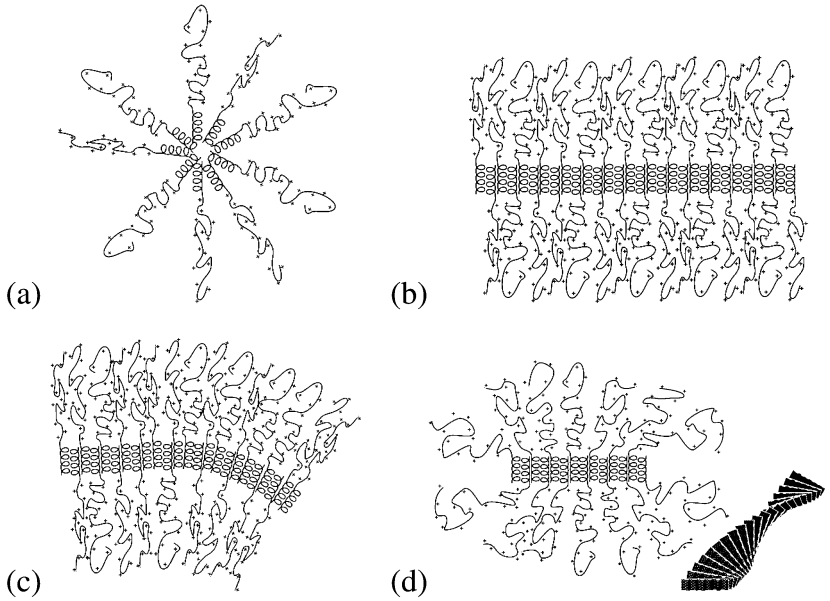

Figure 4. Packing of amphiphilic diblock copolypeptide molecules into (a) spherical micelles, (b) flat membranes, (c) curved membranes, and (d) fibrils, the cross-section being shown in detail and the inset schematically depicting how the cross-sectional layers assemble into twisted fibers (for clarity, only the helices are drawn).

synthesized by functionalizing the lysine monomers with ethylene glycol oligomers.[20] Both blocks of the nonionic block copolypeptides adopt helical conformations, thus giving rise to an amphiphilic rod−rod molecular structure. These molecules prefer to pack in flat lamellar structures or vesicles. As reported in earlier work, such nonionic polypeptides with an overall chain length and hydrophobic block length similar to $K_{160}L_{40}$ did not form hydrogels up to high concentrations.[20]

For the charged lysine-leucine block copolypeptides we therefore need to explore alternative structures to account for hydrogel formation. Candidate structures must be able to form a three-dimensional percolated network by balancing the free energies stemming from the dominant intermolecular interactions and entropic effects introduced above: the hydrophobic attraction between leucine segments, geometry-dependent entropic effects that favor parallel packing of the rodlike helices, the entropy of the polyelectrolyte chains, and repulsive electrostatic forces. Having ruled out spherical micelles (Figure 4a) and flat membranes (Figure 4b) as being too energetically costly, we consider two other plausible candidate packings, sketched in Figure 4c and 4d, to satisfy the energetic tradeoff.

One of the proposed structures is based on introducing curvature of lamellar structures by asymmetrically packing the polyelectrolyte blocks on different sides of the hydrophobic core (Figure 4c). In case of curvature along two orthogonal directions, the volume of the polyelectrolyte corona increases with curvature. The effect is rather subtle: the increase in corona volume is a second-order effect with respect to the ratio of corona thickness to radius of curvature and only relevant for surfaces curved along two directions. Surfaces with curvature along only one direction, that is surfaces with tubular curvature, do not lead to an increase in available volume per polyelectrolyte segment. Connections between curved membranes could give rise to structures that are similar to a closed-cell foam,[21] which would account for gelation at low concentrations. Curvature induces strain on the packing of the hydrophobic helices, although to a much lesser degree than the spherical micelle depicted in Figure 4a. Thus, the geometrical interaction will limit the degree of curvature.

Another possible structure consists of ribbonlike fibrils that are extended in one direction (out-of-paper direction in Figure 4d) but have limited dimensions in the perpendicular direction, the fibril cross-section. In this model, the helices maintain parallel packing while the polyelectrolyte segments maximize their conformational entropy by relaxing laterally, so that the lysine segments in the cross-section exhibit a fanlike structure. Additional entropy can be gained by packing the cross-sectional layers with a twist in the axial direction of the fibrils. Such a packing of the core (see inset of Figure 4d) not only maximizes the volume for the polyelectrolyte segments, it also satisfies the natural tendency toward twisted packing of helical rods.[22,23] There is an energetic penalty associated with assembly in ribbonlike fibrils due to partial exposure of hydrophobic rods at the edges of the fibrils to water. The energetic cost of edge exposure is compensated by the increase in available volume for the polyelectrolytes and by twist along the fiber axis, both of which are impossible in a flat membrane. The width of the fibril is determined by the balance between polyelectrolyte repulsion, hydrophobic edge energy, and the degree of fibril twist, as observed in peptide fibrils formed via β-strand assembly.[22,23] In a fibril framework, both entanglements and branching could yield a percolated network with elastic properties. A network of branched ribbonlike fibrils is in fact similar to open-cell foams.[21]

Electron microscopy and neutron scattering have not provided conclusive quantitative information about the structure on a molecular scale. Cryogenic transmission electron microscopy (CryoTEM) seems to support the coexistence of entangled/branched fibrils and curved membrane-like structures on the molecular scale.[12,15] Most examples in the literature where peptides assemble into ribbonlike fibrils show very well-defined elongated structures using TEM. In those materials, the peptide self-assembly is driven by β-strand formation and the resulting fibrils have highly ordered structures

Table 1. Gelation Concentration and Gel Strength for a Variety of K_mL_n Diblock and $K_mL_nK_m$ Triblock Copolypeptide Architectures

architecture	gelation concentration [wt %]	gel strength [G' at 3 wt %, 1 rad/s]
$K_{90}L_{10}$	no gel at 8%	NA
$K_{80}L_{20}$	no gel at 6%	NA
$K_{180}L_{20}$	2%	12 Pa
$K_{170}L_{30}$	0.75%	590 Pa
$K_{160}L_{40}$	0.25%	4273 Pa
$K_{380}L_{20}$	0.25%	146 Pa
$K_{370}L_{30}$	0.031%	940 Pa
$K_{360}L_{40}$	0.125%	480 Pa
$K_{90}L_{20}K_{90}$	6%	NA
$K_{190}L_{20}K_{190}$	0.5%	501 Pa
$K_{185}L_{30}K_{185}$	0.375%	1035 Pa
$K_{180}L_{40}K_{180}$	0.25%	8650 Pa

due to directional H-bonding between molecules.[11,22,23] The interactions that lead to self-assembly of our amphiphilic block copolypeptides are less specific and more likely to give rise to structures with a broader distribution of shape and size. Although microscopy has been inconclusive in determining the microstructure, it is important to realize that the existence of an open, interconnected structure is essential for gelation at concentrations as low as we have observed for the diblock copolypeptide solutions. In the rest of this paper we focus on systematic changes in the various intermolecular interactions by changing the relative length, number, and composition of blocks in the copolypeptides polymers and use of rheological measurements to extract additional information about the nature of the self-assembly structures.

Tuning Intermolecular Forces: Diblock Architecture. To investigate the gelation mechanism in more detail, sample properties were varied by changing the relative block composition and overall length of the block copolypeptides. Changes in molecular architecture shift the balance between the different molecular interactions and thus provide valuable information about molecular assembly. In Table 1 key rheological information is presented for a large variety of lysine-leucine block copolypeptide architectures. In the next three subsections, the abundance of information in the table will be dissected and elaborated with additional rheological data.

The rheology of all polypeptides was measured as a function of concentration (see Figure 2). Noting that above the concentration where the samples gel the value of the elastic modulus G' is practically independent of angular frequency, we focused on the viscoelastic properties at one particular frequency ($\omega = 1$ rad/s) to represent gel strength. Consistent with this focus on one frequency, we defined the gelation threshold as the concentration ϕ_{gel} for which the ratio of elastic and loss modulus $G'/G'' = 1$, measured at 1 rad/s. Below ϕ_{gel}, viscous properties are dominant and $G'/G'' < 1$; above ϕ_{gel} elastic properties dominate and $G'/G'' > 1$. In Figure 5 we summarize the gelation characteristics for a number of K_nL_m diblock copolypeptides by presenting the ratio of dynamic moduli as a function of concentration. The "gelation concentration" in Table 1 refers to the lowest concentration at which we found $G'/G'' > 1$.

In previously published work[12] it was shown that the presence of an ordered chain conformation (α-helix or β-sheet) in the hydrophobic block was crucial to gelation at low concentrations. Loss of secondary structure compromised packing of the hydrophobic segments into

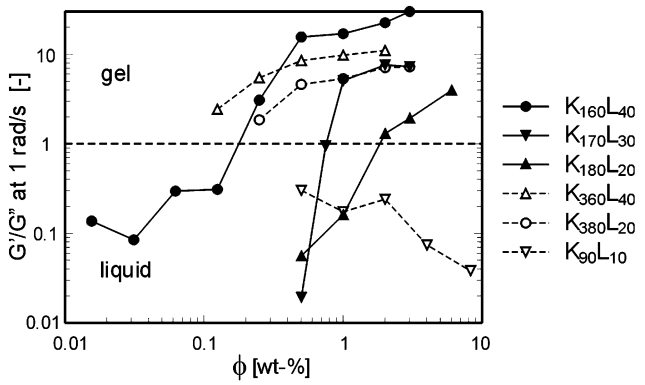

Figure 5. Gelation of a variety of K_nL_m diblock copolypeptides as a function of polypeptide concentration; sample properties are represented by the ratio G'/G'' of storage to loss modulus at 1 rad/s. $G'/G'' < 1$ indicates liquidlike properties, while $G'/G'' > 1$ characterizes a gel.

membranes or fibrils of high structural integrity and strength. The geometry of the hydrophobic block guides the self-assembly process. Increasing the length of the hydrophobic block also had dramatic effects. Changing the relative lengths of the hydrophobic and hydrophilic blocks from $K_{180}L_{20}$ to $K_{170}L_{30}$ and then to $K_{160}L_{40}$, the overall size of the copolypeptide does not change. Nevertheless, ϕ_{gel} drops by an order of magnitude from 2.0 to 0.25 wt % and the gel strength, defined in Table 1 as the value of G' at 1 rad/s in a 3.0 wt % solution, increases from 12 to 4300 Pa.

Figure 6 presents the oscillatory rheology (frequency and strain amplitude sweeps) for these three copolypeptides at 3.0 wt % in more detail. All three are in the gel regime ($c > \phi_{gel}$) at this particular concentration, although $K_{180}L_{20}$ at 3.0 wt % is only just above its gelation threshold. This large change in ϕ_{gel} resulting from relatively small changes in polypeptide architecture is sensible when viewed in light of the structures sketched in Figure 4. If the self-assembly is driven by ordered packing of the hydrophobic domains, increasing the length of the leucine segments should strengthen both hydrophobic and geometric interactions. There are practical limits to the length of the hydrophobic block: if the number of leucine monomers is larger than about 60, the hydrophobicity becomes so strong that the diblock copolypeptides are rendered insoluble in water.

The strain amplitude sweeps in Figure 6b also provided information on self-assembly structure: the strongest gel former, $K_{160}L_{40}$, possessed a brittle structure, indicated by a sudden decrease of G' over a narrow range of strain amplitudes around $\gamma_0 = 0.01$. $K_{180}L_{20}$, on the other hand, shows more complex nonlinear behavior. After the onset of nonlinearity at $\gamma_0 = 0.5$, the sample displays strain hardening, becoming stronger with increasing strain amplitude before the gel finally breaks down around $\gamma_0 = 2.0$. The strain hardening and more gradually occurring nonlinearity suggest that for $K_{180}L_{20}$ the self-assembled structure is locked into place less rigidly than for $K_{160}L_{40}$: the $K_{180}L_{20}$ structure can be deformed to a larger extent before it yields.

Table 1 illustrates the importance of the polyelectrolyte segment for stabilizing the self-assembled structures. For example, $K_{80}L_{20}$ did not form a gel even up to 6.0 wt % even though this sample possesses a helical hydrophobic segment of the same length as $K_{180}L_{20}$. A certain minimum length of the poly-L-lysine is required to induce gelation: the 200-mer block copolypeptides

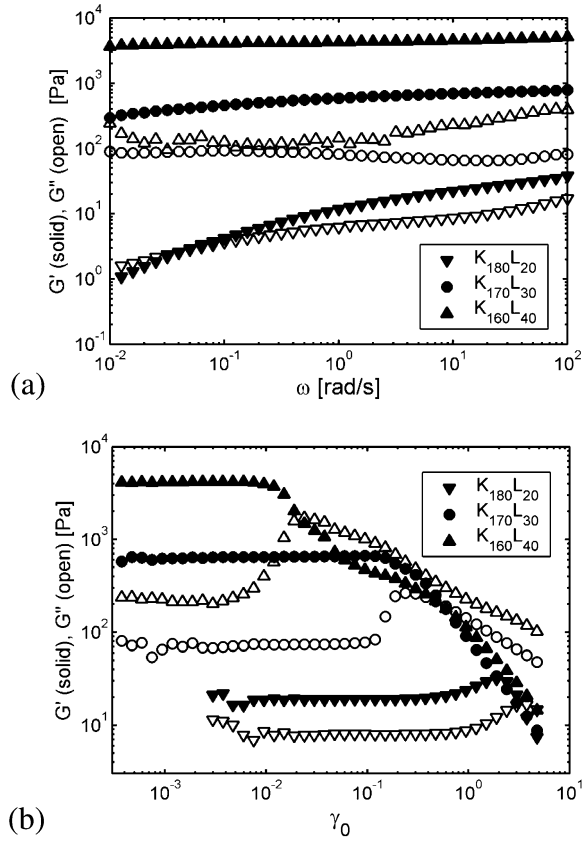

Figure 6. (a) Storage modulus G' (solid symbols) and loss modulus G'' (open symbols) as a function of angular frequency for three different block copolypeptides with the same overall length at 3 wt %: (▼) $K_{180}L_{20}$, (●) $K_{170}L_{30}$, and (▲) $K_{160}L_{40}$; (b) Strain sweeps for the same samples at angular frequency ω = 6 rad/s.

meet this criterion. A further increase of copolypeptide length to 400-mer provides further stabilization of the self-assembly and leads to significantly lower gelation concentrations, which is remarkable since the number density of hydrophobic segments at a given concentration by weight is twice as low for a 400-mer in comparison with a 200-mer block copolypeptide. The hypothetical structures of Figure 4 are consistent with this observation, since we argued that polyelectrolyte repulsion is essential for the formation of a percolated gel network.

The strength of the 400-mer block copolypeptide gels at the standardized concentration of 3.0 wt % emphasizes how delicate the balance between repulsion and attraction is. $K_{380}L_{20}$ is much stronger than $K_{180}L_{20}$, while $K_{360}L_{40}$ is actually weaker than $K_{160}L_{40}$ at the same polymer concentration. $K_{370}L_{30}$ exhibits gelation at extremely low concentrations. However, lower gelation concentrations ϕ_{gel} do not automatically result in higher gel strength. One must keep in mind that the comparison of polypeptides of different molecular weights at a standardized weight fraction of 3.0% implies that the number of molecules per unit volume varies.

Specificity of Self-Assembly: Mixing Experiments. The variations between molecular architectures revealed important information about the gel formation in our unique block copolypeptides. To obtain a more thorough understanding of the nature of the intermolecular interactions, we performed a variety of additional experiments employing mixtures of different block copolypeptides. The controlled manipulation of sample composition enabled us to probe the subtleties of block copolypeptide self-assembly in more detail.

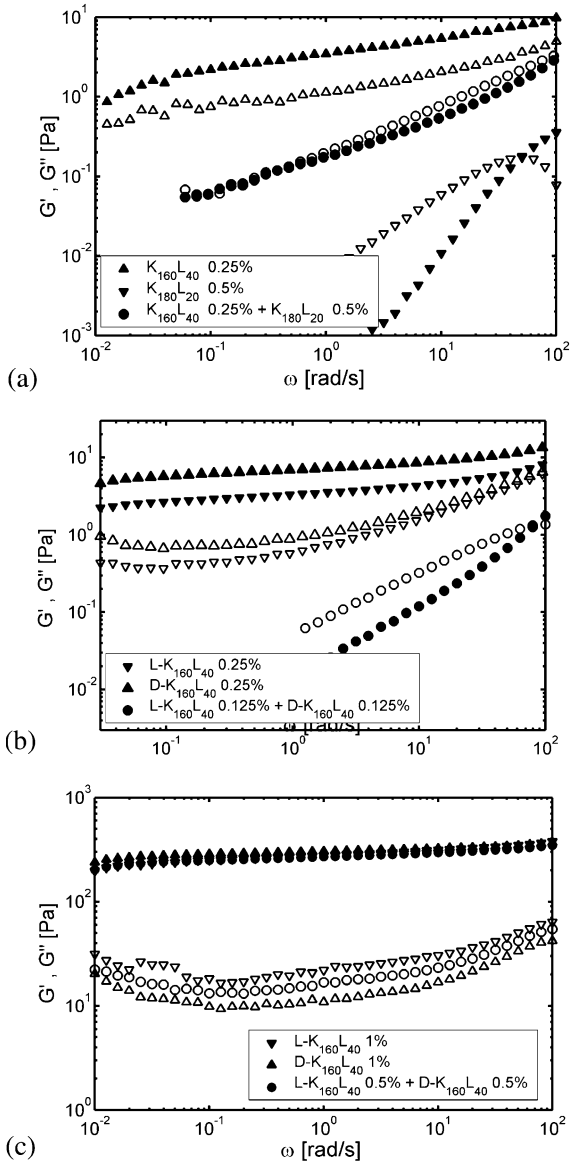

Figure 7. Storage modulus G' (solid symbols) and loss modulus G'' (open symbols) as a function of angular frequency for pure samples and mixtures with different leucine segments. (a) (▲) 0.25 wt % $K_{160}L_{40}$, (▼) 0.5 wt % $K_{180}L_{20}$, and (●) mix with 0.25 wt % $K_{160}L_{40}$ and 0.5 wt % $K_{180}L_{20}$; (b) (▼) 0.25 wt % $K_{160}L_{40}$, (▲) 0.25 wt % D-$K_{160}L_{40}$, and (●) mix with 0.125 wt % $K_{160}L_{40}$ and 0.125 wt % D-$K_{160}L_{40}$; (c) (▼) 1 wt % $K_{160}L_{40}$, (▲) 1 wt % D-$K_{160}L_{40}$, and (●) mix with 0.5 wt % $K_{160}L_{40}$ and 0.5 wt % D-$K_{160}L_{40}$.

The first experiment involved mixing $K_{160}L_{40}$ and $K_{180}L_{20}$, diblock copolypeptides of the same overall length but with different leucine-to-lysine ratios. The results are displayed in Figure 7a. At a concentration of 0.25 wt %, a pure $K_{160}L_{40}$ solution is just above ϕ_{gel} and forms a weak gel, while a pure 0.50 wt % $K_{180}L_{20}$ solution is liquidlike. Surprisingly, a sample that contains both block copolypeptides at these concentrations is also liquidlike. Apparently, the $K_{160}L_{40}$ structure that exists in the pure 0.25 wt % solution loses its integrity due to the presence of added $K_{180}L_{20}$ molecules. This observation can only be explained if the two molecular species self-assemble together in structures of mixed composition with a lower ϕ_{gel} than the $K_{160}L_{40}$ structures. If phase separation had occurred into two popula-

tions of $K_{160}L_{40}$ and $K_{180}L_{20}$ assemblies, one would expect the mixture to be at least as strong as the pure $K_{160}L_{40}$ sample. For the hypothetical structures sketched in Figure 4c and 4d, it can easily be imagined that the inclusion of short L_{20}-segments into the $K_{160}L_{40}$-based structure compromise the packing of the helical rods in the hydrophobic core, thereby suppressing gel formation.

Similar results were observed for $K_{160}L_{40}$ and K_{160}-(rac-L)$_{40}$, which have the same molecular composition but a different secondary structure in the hydrophobic segment. The mixture containing 0.25 wt % of each species (0.50 wt % in total) was liquidlike, while the pure 0.25 wt % $K_{160}L_{40}$ sample was a gel. The lack of secondary structure in the K_{160}(rac-L)$_{40}$ molecules seemingly disrupts the packing of $K_{160}L_{40}$ similar to the short segments of $K_{180}L_{20}$. To summarize, it can be said that the self-assembly process is highly sensitive to sample composition: the presence of molecules that disrupt the packing of the leucine blocks has adverse effects on gel formation. A narrow size distribution of the hydrophobic segment is instrumental for the formation of hydrogels at low concentration.

In a second set of experiments we studied the effect of chirality on self-assembly by comparing the gelation behavior of $K_{160}L_{40}$ (blocks of L-lysine and L-leucine) and D-$K_{160}L_{40}$ (D-lysine and D-leucine). These experiments were designed to probe the sensitivity of the self-assembly to subtleties in the helical packing. Analogous to left- and right-handed screws, helices of opposite chirality are unable to pack as closely as helices of identical chirality.

As might be expected, in enantiomerically pure samples the self-assembly properties are insensitive to chirality. Both copolypeptides have nearly identical gelation properties: $\phi_{gel} = 0.25$ wt % and elastic modulus of 276 Pa ($K_{160}L_{40}$) and 304 Pa (D-$K_{160}L_{40}$) for 1.0 wt % gels at 1 rad/s. The small difference in strength can be attributed to variations in molecular composition due to synthesis. The sensitivity of gel strength to slight variations in leucine segment length was highlighted in the previous section where we compared $K_{160}L_{40}$ and $K_{170}L_{30}$.

Despite the similarities between pure block copolypeptide solutions, equimolar mixtures of the enantiomers behaved noticeably differently, in particular close to the gelation threshold, as shown in Figure 7b and 7c. The gelation concentration ϕ_{gel} for the mixture was 0.50 wt % in contrast to $\phi_{gel} = 0.25$ wt % for the individual polypeptides. A mixture with 0.125 wt % of each species (0.25 wt % in total) was liquidlike, while pure solutions of the L- and D-enantiomer were weak gels at the same total polypeptide concentration (Figure 7b).

At higher concentrations, well above ϕ_{gel}, the situation changed and the mixture had virtually the same rheological properties as the enantiomerically pure solutions (see Figure 7c): at 1.0 wt %, $G' = 269$ Pa at 1 rad/s for the racemic mixture, which is comparable to the values given above for the enantiomerically pure solutions. The method of sample preparation had no impact: dissolving the copolypeptide powders together or mixing predissolved pure copolypeptide solutions yielded the same results.

The experiments show that mixtures of left- and right-handed helical rods do not assemble as effectively as pure systems. The elevated gelation concentration of the equimolar mixture seems to imply that the racemic gel consists of two different populations of predominantly L- and D-structures, which are then mixed on a mesoscopic level. This would explain why the gelation of the left- and right-handed molecules is noncooperative. As a result, 0.25 wt % of each species is needed for gel formation in the equimolar racemic mixture, double the amount for the pure samples. Once the gelation threshold has been passed, the network composed of left- and right-handed structures behaves similar to an enantiomerically pure solution. Although rheological data do not provide unambiguous proof for this phase-separated scenario, it is evident that even subtle features such as helical chirality have an impact on the self-assembly of the hydrophobic segments. These experiments therefore support the hypothesis of twisted fibrils, which are expected to be more sensitive to chirality than curved membranes.

The final mixing experiments focused on the role of the hydrophilic polyelectrolyte segments by mixing samples with the same hydrophobic poly-L-leucine block length but with hydrophilic poly-L-lysine segments of different lengths. The starting point for the experiments was a 2.5 wt % $K_{180}L_{20}$ solution with gellike properties. Mixtures were prepared by replacing 20% of the $K_{180}L_{20}$ molecules by either $K_{380}L_{20}$ or $K_{80}L_{20}$. To achieve the 4:1 molar ratio, 0.50 wt % $K_{180}L_{20}$ was replaced with 1.0 wt % $K_{380}L_{20}$ or 0.25 wt % $K_{80}L_{20}$, respectively, to account for the differences in molecular weight. A pure 1.0 wt % $K_{380}L_{20}$ solution is a gel ($G' = 41$ Pa at 1 rad/s), while the 0.25 wt % $K_{80}L_{20}$ solution has rheological properties that are virtually indistinguishable from pure water, the steady-shear viscosity being 1.02 mPa·s at 23.5 °C.

Figure 8a shows the results of oscillatory frequency sweeps. In contrast to the previous experiments that described mixtures of molecules with different leucine segments, mixing molecules with different poly-L-lysine blocks did not break down the gel structure: both mixtures are gels. Although the addition of $K_{80}L_{20}$ weakened the gel, it did not compromise the structure to the point of breakage. Replacing 20% of the molecules in the $K_{180}L_{20}$ gel with $K_{380}L_{20}$ significantly increased the gel strength. One of the benefits of mixing is presented in Figure 8b, where the strain amplitude sweeps are presented for the $K_{180}L_{20}/K_{380}L_{20}$ mixture and pure samples of the same block copolypeptides. Mixing in a small fraction of molecules with long polyelectrolyte segments strengthens the gel while maintaining the toughness of the $K_{180}L_{20}$ assembly, which is reflected by the higher critical strain value at which the sample breaks down.

The mixing results support the hypothesis that gel formation is predominantly driven by the formation of packed hydrophobic cores. Mixing noncompatible molecules with opposite helical chirality, different length, or loss of secondary structure in the poly-L-leucine block has a negative impact on molecular self-assembly. On the other hand, mixing molecules with different hydrophilic polyelectrolyte segment lengths leads to more subtle changes in gel properties by tuning the repulsive forces. For materials design purposes, this mix-and-match methodology offers additional opportunities to optimize block copolypeptide hydrogel properties for specific applications.

Triblock Architecture. In an attempt to shed more light onto the nature of the self-assembly structure and discriminate between membranes and fibrils, we also synthesized and characterized triblock copolypeptides

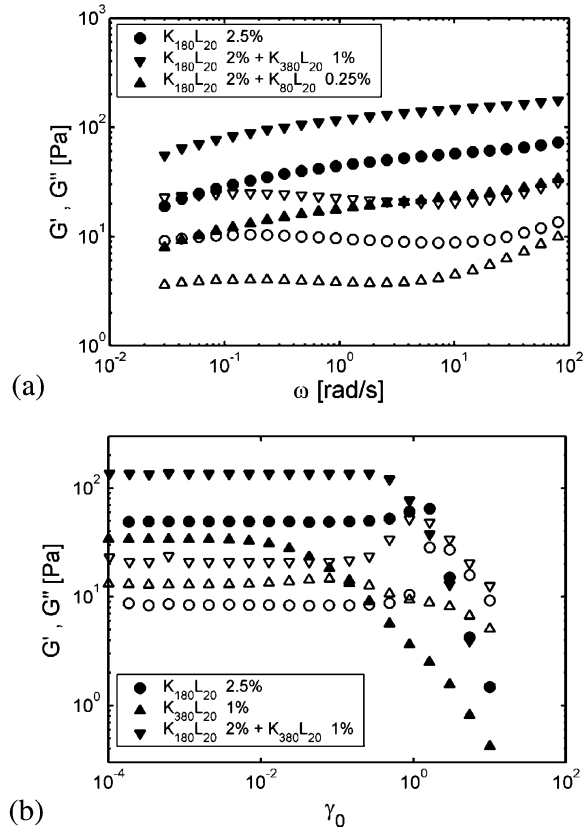

Figure 8. Storage modulus G' (solid symbols) and loss modulus G'' (open symbols) for pure samples and mixtures with different lysine segment lengths: (a) frequency sweep of (●) 2.5 wt % $K_{180}L_{20}$, (▼) mix with 2 wt % $K_{180}L_{20}$ and 1 wt % $K_{380}L_{20}$, and (▲) mix with 2 wt % $K_{180}L_{20}$ and 0.25 wt % $K_{80}L_{20}$; (b) strain amplitude sweep at 6 rad/s of (●) 2.5 wt % $K_{180}L_{20}$, (▲) 1 wt % $K_{380}L_{20}$, and (▼) mix with 2 wt % $K_{180}L_{20}$ and 1 wt % $K_{380}L_{20}$.

with a hydrophobic core and two hydrophilic segments (Figure 1b). The molecular symmetry due to covalent coupling of polyelectrolyte blocks on both ends of the hydrophobic helix renders it impossible to assemble in asymmetrical, curved membrane structures (Figure 4c). The fibril structure (Figure 4d) should not be destabilized by the presence of the second poly-L-lysine segment. On the contrary, the increased packing density of polyelectrolyte chains onto the hydrophobic core should amplify the need for lateral relaxation, thus leading to smaller fibril width and a larger degree of twist (shorter pitch) in the axial direction. A decrease of the fibril width results in an increase of fibril length per unit volume if the polypeptide concentration remains the same. As a result, one might expect a lower gelation concentration. In addition, individual triblock fibrils should be more rigid than their diblock equivalents of the same fibril width owing to the higher density of the polyelectrolyte corona and the resulting increase in bending modulus.

Table 1 shows, indeed, that triblock architectures are very efficient gel formers with respect to both gel strength and gelation concentration. As observed for the diblocks, the length of the polyelectrolyte block must meet a certain minimum length before gelation takes place: $K_{90}L_{20}K_{90}$ did not form gels until 6.0 wt % of material was added to the solution, while $K_{190}L_{20}K_{190}$ formed gels at only 0.50 wt %. The effect of lengthening the hydrophobic block on gelation concentration was not quite as dramatic for triblock designs as it was for the diblock systems. The change in gelation concentration was less pronounced: from 0.50 wt % for $K_{190}L_{20}K_{190}$ to 0.25 wt % for $K_{180}L_{40}$ K_{180}, while a similar change in leucine segment length for the diblocks resulted in a factor 8 reduction of the gelation threshold. The effect of changing the hydrophobic block length on gel strength was still quite impressive, as seen with the diblocks. These results hint that the parameters controlling gel formation and strength in both diblock and triblock copolypeptides are similar. Hence, it is likely that the self-assembled structure of the gel network is also similar for both these materials.

Nanoscale Structure. We have been unable to determine the exact structure of the self-assembled amphiphilic block copolymers, either for the diblocks or triblocks. It is clear that the gel-forming block copolypeptides do not form spherical micelles or flat lamellar structures, both from cryoTEM pictures and because these structures are simply not capable of forming a percolated network at 0.25 wt % polypeptide concentrations.

The two most likely alternatives, curved membranes and fibrils, could both account for the low gelation thresholds ϕ_{gel}. One-dimensional fibrils are more efficient for network formation in the form of open-cell foams or entangled fibrils than two-dimensional membranes, which have to assemble to closed-cell foams. The results for triblock copolypeptides and racemic mixtures described above favor the existence of fibrils rather than curved membranes. However, this does not automatically imply that all diblock copolypeptide designs necessarily assemble into the same structure or that the dimensions of the assembly (e.g., fibril width) are monodisperse throughout the solution. Unfortunately, cryoTEM and neutron scattering experiments have not been able to provide unambiguous proof; they leave open the possibility of coexistence of curved membranes and fibrils, the balance seemingly shifting more toward fibrils for some block copolypeptides.[15] As a result, quantitative modeling and analysis of the rheological results in terms of molecular structure is difficult.

In the literature theoretical predictions are available for the scaling of elastic plateau modulus G' as a function of concentration for cross-linked and entangled networks of semi-flexible polymers and cellular solids.[21,24] The semi-flexible polymer theory was developed for actin networks and predicts $G' \approx \phi_f^{11/5}$ for entangled networks and a slightly higher exponent $G' \approx \phi_f^{5/2}$ for densely cross-linked actin networks, ϕ_f being the filament concentration. If our block copolypeptides do indeed form fibrils, they should be rather stiff due to the closely packed geometry of the hydrophobic core and thus resemble semi-flexible polymers. In Figure 9 we plotted the gel strength for a number of block copolypeptides as a function of polypeptide concentration ϕ to study the scaling behavior of G'. Once again we use the value of G' at 1 rad/s as a measure for the plateau value. For strong hydrogels (e.g., $K_{160}L_{40}$ at 3.0 wt %, Figure 6) this approximation is very reasonable. In other samples the elastic modulus G' has not reached a constant value at an angular frequency of 1 rad/s, and thus, the approximation underestimates the plateau value; in general, this occurs for samples just above the gelation threshold, for example, $K_{180}L_{20}$ at 3.0 wt % (Figure 6). We only have data over a limited range of concentrations to test the exponential scaling predictions. Considering these limitations, the scaling is in

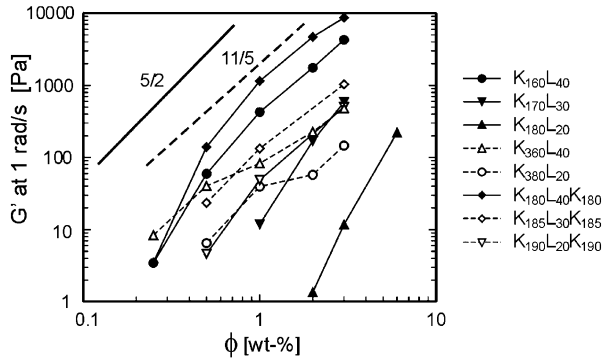

Figure 9. Gel strength of block copolypeptide hydrogels as a function of concentration, represented by G' at 1 rad/s. The lines are theoretical scaling predictions for entangled solutions (dashed) and cross-linked networks (solid) of semiflexible fibers.[24]

reasonable agreement with the entangled fibril model, in particular for block copolypeptides that form hydrogels at the lowest concentrations. One possible explanation for the discrepancies is that in actin solutions addition of actin monomer automatically leads to added fiber length, since the width of actin filaments is defined by the monomer dimensions. As a result, a linear relation exists between the actin concentration and the fiber length present in the sample. For our block copolypeptides, however, the width of the ribbonlike fibrils is not defined by specific interactions and it is therefore quite possible that the width of the ribbons depends slightly on polypeptide concentration ϕ, which would then affect the scaling exponent α of $G' \approx \phi^{\alpha}$.

If the self-assembled structure is constructed from two-dimensional curved membranes, the network must be similar to foams. For foams (also referred to as cellular solids), the general scaling relation between elastic modulus and concentration is given by: $G' \approx (1 - \epsilon)^2(\rho_{tot}/\rho_w)^2 + \epsilon(\rho_{tot}/\rho_w)$.[21] In this equation the concentration of foam material is defined as the relative density (ρ_{tot}/ρ_w), where ρ_{tot} is the macroscopically averaged density of the foam and ρ_w the density of wall material. If the density of the gas phase can be neglected in comparison with the wall material, ρ_{tot}/ρ_w is the volume fraction of wall material. In our hydrogels, the polypeptide volume fraction is equal to the weight fraction ϕ, if the density of the copolypeptide structures is close to that of water. The other important scaling parameter is ϵ, the fraction of material in the foam that is incorporated in the cell walls. The remaining fraction $(1 - \epsilon)$ represents the amount of material in the Plateau borders, the areas where curved membranes connect. For many foams, wall material is concentrated in these Plateau borders, so that $\epsilon \ll 1$. However, if our block copolypeptides self-assemble in membranes (Figure 4c), the thickness of these membranes is set by molecular design and limited. As a consequence, the volume of polypeptide material that can be stored in the Plateau borders is restricted and $\epsilon \approx 1$, if the block copolypeptides assemble in a *closed-cell* foam. In *open-cell* foams there are no membranes to constitute the cell walls, only interconnected plateau borders, and thus $\epsilon = 0$.

Application of the above relation for cellular solids to the block copolypeptide structures then leads to the scaling prediction $G' \approx \phi$ for foamlike structures of curved membranes at low volume fraction. Figure 9 clearly shows that the scaling is far from linear over the range of experimental data. For the open-cell foam the scaling reduces to $G' \approx \phi^2$. Not surprisingly, this quadratic scaling is very close to the prediction for a branched fiber network, which gives $G' \approx \phi^{2.5}$.

Our data are not clear enough to distinguish between the open-cell and fiber network models, both of which consist in essence of interconnected fibers or ribbonlike structures. On the other hand, the foam model eliminates the hypothesis of a closed-cell foam of curved, two-dimensional membranes (Figure 4c), since that concept is inconsistent the observed scaling behavior.

If the strength of the hydrogels indeed originates from the presence of ribbonlike structures, either in an open-cell foam or an entangled fibril network, the modulus of the gel can be expected to scale as $G' \approx \kappa^2$, κ being the bending modulus of an individual fiber.[24,25] Assuming that the closely packed hydrophobic core is the primary source of bending rigidity and that the ribbonlike fibrils have a rectangular cross-section (Figure 4d), equations from basic static mechanics[26] can be used to estimate κ. If the fibril has width W and thickness H, there are two orthogonal bending moduli that, respectively, scale like $\kappa_1 \approx H^3W$ and $\kappa_2 \approx W^3H$. Since the spatial orientation of the fibrils in the hydrogel network is random, the strength of the network is expected to be determined by the smallest of the two bending moduli; in the case of $W > H$, this is κ_1 and consequently $G' \approx H^6W^2$.

Direct comparison of these simple model predictions with rheological data is complicated by the fact that the fibril dimensions H and W cannot be manipulated independently in a controlled way. In the self-assembled structure proposed in Figure 4d, the fibril thickness H scales linearly with the number of monomers m in the hydrophobic block L_m and can be manipulated through synthesis. However, as noted before, the width W is then determined by the delicate balance of the intermolecular forces and cannot be measured or predicted quantitatively at this point. Thus, the only meaningful experimental validation of the scaling relation comes from comparing hydrogels with molecular architectures that lead to similar fibril width for different values of H. The best candidates in this study for such a comparison are the diblock pair $K_{170}L_{30}$ and $K_{160}L_{40}$ and the triblock pair $K_{185}L_{30}K_{185}$ and $K_{180}L_{40}L_{180}$. All four block copolypeptides are strong gel formers. If we assume that the fibril width W is the same for both entities of each pair, increasing the hydrophobic block length m from 30 to 40 mers leads to a model-predicted increase of G' by a factor $(4/3)^6 = 5.6$. This is remarkably close to the experimentally observed factor 7.2 increase of G' at 1 rad/s between $K_{170}L_{30}$ and $K_{160}L_{40}$ at 3 wt % (see Table 1) as well as the factor 8.4 increase for $K_{185}L_{30}K_{185}$ and $K_{180}L_{40}L_{180}$ at the same concentration and frequency. The deviations between model and experiment can easily be attributed to experimental uncertainty in the block length m ($G' \approx m^6$) and to slight variations in the fibril width W. Unfortunately, lack of knowledge about the fibril dimensions forces us to restrict validation of the scaling relation to a few samples with similar self-assembled structures, as concluded from their rheological characteristics; for these cases the model works surprisingly well. The block copolypeptides with hydrophobic block lengths of 20 mers (Table 1) do not follow the scaling predictions; however, these molecular architectures are close to the critical limit of m that is required for gel formation.

Although this analysis does not provide conclusive evidence about the precise nature of the self-assembled network structure, it yields valuable indirect support to the proposed ribbonlike assembly.

IV. Conclusions

Amphiphilic block copolypeptides, a new class of synthetic materials with biomimetic features, exhibit remarkable gelation properties in aqueous solution. They form strong hydrogels at low polypeptide concentrations. Systematic analysis of the rheology for different molecular architectures of lysine-leucine block copolypeptides has provided insight in the self-assembly process.

The dominant driving force toward aggregation is the hydrophobicity of poly-leucine segments. Polyelectrolyte poly-L-lysine blocks provide solubility and counteract aggregation of the hydrophobes. Low gelation concentrations indicate that diblock copolypeptides do not assemble into spherical micelles such as most amphiphilic block copolymers. The scaling behavior of gel strength with polypeptide concentration supports the hypothesis that the gels consist of a network of ribbonlike structures, which are the result of geometrical packing constraints resulting from the unique rodlike nature of the helical leucine blocks. To satisfy these limitations the amphiphilic molecules most likely aggregate into twisted fibrils with a core of closely packed hydrophobic helices and a polyelectrolyte corona. The mechanical strength of the network originates either from entanglements, branching, or a combination of these mechanisms, which could not be clarified by rheological experiments. Symmetrical triblock copolypeptides with a hydrophobic leucine center and polyelectrolyte lysine blocks on either side formed hydrogels at even lower concentrations than analogous diblocks. The rheology of the triblock samples was comparable to the diblocks, which implies that the self-assembled structures are similar as well.

For both di- and triblock architectures, increasing the length of the hydrophobic block at constant overall polypeptide length lowers the gelation concentration, strengthens the gel dramatically, and makes the assembled structure more brittle. Enlarging the polyelectrolyte segment at a constant hydrophobe length also lowers the gelation concentration, but the effect on gel strength is less pronounced. These observations are in agreement with the proposed twisted fibril model. The polyelectrolyte segments are instrumental for fibril formation by preventing packing of the helices in flat membranes. The poly-L-lysine block must have a minimum length of between 100 and 150 monomers to induce fibril formation. The lateral dimension of the fibrils determines the gelation threshold, with narrower fibrils leading to lower gelation concentrations. The hydrophobic block, on the other hand, predominantly determines gel strength through the stiffness of the core.

Mixing experiments emphasized the specificity of self-assembly. The packing of the hydrophobic blocks was disrupted in samples with mixtures of block copolypeptides with a different length, chirality, or secondary structure in the poly-leucine segment. Bidispersity in the polyelectrolyte block affected the hydrogel properties in a more subtle way. Mixtures of molecules with different hydrophilic block lengths combined beneficial mechanical properties of the individual block copolypeptide components.

In conclusion, block copolypeptides were found to gel efficiently in aqueous solution. The flexibility of the block copolypeptide synthesis, which enables the inclusion of amino acids with specific (bio)chemical properties, and sensitivity of self-assembly to small variations in molecular architecture facilitate the design of new polypeptide hydrogels with tunable mechanical properties and functionality for specific applications.

Acknowledgment. This work was supported by grants from the National Science Foundation (Chemical and Transport Systems CTS-9986347 and MRSEC Program DMR-0080034). V.B. thanks The Netherlands Organization for Scientific Research (NWO) for a Talent-grant. We thank Dr. Jerry Hu (MRL, UCSB) for assistance with NMR experiments.

References and Notes

(1) Bhatia, S. R.; Mourchid, A.; Joanicot, M. *Curr. Opin. Colloid Interface Sci.* **2001**, *6*, 471.
(2) Larson, R. G. *The structure and rheology of complex fluids*; Oxford University Press: New York, 1999.
(3) Fredrickson, G. H.; Bates, F. S. *Annu. Rev. Mater. Sci.* **1996**, *26*, 501.
(4) *Amphiphilic block copolymers: self-assembly and applications*; Alexandridis, P., Lindman, B., Eds.; Elsevier Science: Amsterdam, 2000.
(5) Israelachvili, J. N. *Intermolecular and surface forces*, 2nd ed.; Academic Press London: London, 1992.
(6) Alexandridis, P.; Olsson, U.; Lindman, B. *Langmuir* **1998**, *14*, 2627.
(7) Deming, T. J. *J. Polym. Sci. Polym. Chem.* **2000**, *38*, 3011.
(8) Deming, T. J. *Nature* **1997**, *390*, 386.
(9) Wang, C.; Stewart, R. J.; Kopecek, J. *Nature* **1999**, *397*, 417.
(10) Petka, W. A.; Harden, J. L.; McGrath, K. P.; Wirtz, D.; Tirrell, D. A. *Science* **1998**, *281*, 389.
(11) Goeden-Wood, N. L.; Keasling, J. D.; Muller, S. J. *Macromolecules* **2003**, *36*, 2932.
(12) Nowak, A. P.; Breedveld, V.; Pakstis, L.; Ozbas, B.; Pine, D. J.; Pochan, D.; Deming, T. J. *Nature* **2002**, *417*, 424.
(13) Hamley, I. W.; Daniel, C.; Mingvanish, W.; Mai, S. M.; Booth, C.; Messe, L.; Ryan, A. J. *Langmuir* **2000**, *16*, 2508.
(14) Buitenhuis, J.; Forster, S. *J. Chem. Phys.* **1997**, *107*, 262.
(15) Pochan, D. J.; Pakstis, L.; Ozbas, B.; Nowak, A. P.; Deming, T. J. *Macromolecules* **2002**, *35*, 5358.
(16) Tsitsilianis, C.; Iliopoulos, I.; Ducouret, G. *Macromolecules* **2000**, *33*, 2936.
(17) Winnik, M. A.; Yekta, A. *Curr. Opin. Colloid Interface Sci.* **1997**, *2*, 424.
(18) Clark, A. C.; Ross-Murphy, S. B. *Adv. Polym. Sci.* **1987**, *83*, 57.
(19) Breedveld, V.; Pine, D. J. *J. Mater. Sci.* **2003**, *38*, 4461.
(20) Yu, M.; Nowak, A. P.; Deming, T. J.; Pochan, D. J. *J. Am. Chem. Soc.* **1999**, *121*, 12210.
(21) Gibson, L. J.; Ashby, M. F. *Cellular solids: structure and properties*, 2nd ed.; Cambridge University Press: Cambridge, 1997.
(22) Lashuel, H. A.; LaBrenz, S. R.; Woo, L.; Serpell, L. C.; Kelly, J. W. *J. Am. Chem. Soc.* **2000**, *122*, 5262.
(23) Aggeli, A.; Nyrkova, I. A.; Bell, M.; Harding, R.; Carrick, L.; McLeish, T. C. B.; Semenov, A. N.; Boden, N. *Proc. Natl. Acad. Sci. U.S.A.* **2001**, *98*, 11857.
(24) MacKintosh, F. C.; Kas, J.; Janmey, P. A. *Phys. Rev. Lett.* **1995**, *75*, 4425.
(25) Rabin, Y. Personal communication, 2002.
(26) Beer, F. P.; Johnston, E. R. *Mechanics of materials*; McGraw-Hill: New York, 1981.

MA049885F